Adaptive strain prompting a pseudo-morphotropic phase boundary in ferroelectric (1-x)Na_{0.5}Bi_{0.5}TiO_{3}-xBaTiO_{3}

K. Datta, R. B. Neder, A. Richter, M. Göbbels, J. C. Neuefeind, and B. Mihailova

Phys. Rev. B **97**, 184101 — Published 3 May 2018

DOI: 10.1103/PhysRevB.97.184101

Adaptive strain prompting a 'pseudo' morphotropic phase boundary in ferroelectric (1-x)$Na_{0.5}Bi_{0.5}TiO_3$-$x$$BaTiO_3$

K. Datta,[1] R. B. Neder,[2] A. Richter,[3] M. Göbbels,[3] J. C. Neuefeind,[4] and B. Mihailova[1]

[1] *Department of Earth Sciences, University of Hamburg, Hamburg - 20146, Germany.*[*]
[2] *Department of Crystallography and Structure Physics, Friedrich-Alexander-Universität Erlangen-Nürnberg, Staudtstrasse 3, Erlangen - 91058, Germany.*
[3] *Mineralogy, GeoZentrum Nordbayern, Friedrich-Alexander-Universität Erlangen-Nürnberg, Schlossgarten 5a, Erlangen - 91054, Germany.*
[4] *Chemical and Engineering Materials Division, Oak Ridge National Laboratory, Oak Ridge, Tennessee - 37831, United States.*

Understanding of atomistic origin of morphotropic phase boundary (MPB) occurring in composition-temperature phase diagrams of ferroelectric solid solutions is a key topic in material science because materials exhibit anomalous properties at the MPB. Here we reveal mesoscopic-scale structural correlations for a leading Pb-free ferroelectric system (1-x)$Na_{0.5}Bi_{0.5}TiO_3$-$x$$BaTiO_3$ (NBT-xBT) by examining atomic pair distribution functions (PDFs) and Raman scattering data at ambient conditions. We demonstrate that the amplification of piezoelectric properties of NBT-xBT at the MPB are predominantly driven by an easy switchability resulting from a progressive decoupling between strain and polarization as the Ba-content enhances from zero to the critical MPB composition. It was observed that as Ba-content increases towards MPB, competing local correlations, such as A-site chemical order, antiferrodistortive correlations of correlated BO_6 tilts, and antipolar Bi shifts, are reduced, which in turn render favorable conditions for easy switching of local dipoles under external fields. In addition, the evolving characteristics of the atomic dynamics as a function of composition suggest that the local potential functions of the cations are not completely flat at the MPB. Altogether our results reveal atomistic mechanisms responsible for the observed elevated MPB-properties in the case of NBT-xBT which imply that the so-called 'MPB' of NBT-xBT should not be categorized as originally introduced for Pb-containing solid solutions.

I. INTRODUCTION

Ferroelectrics with switchable spontaneous polarization and inherent ability to convert electrical energy to mechanical energy and vice versa, find numerous applications in modern electronic devices ranging from non-volatile memories to sensors in aeronautical applications. Currently, industrial ferroelectric materials are limited to Pb-containing solid solutions, such as $PbZr_xTi_{1-x}O_3$ (PZT), which shows excellent electromechanical properties including good stability over a wide range of operation temperatures, especially in the vicinity of a composition-driven structural phase boundary, known as morphotropic phase boundary (MPB)[1]. However, in the light of present directives of promoting environmentally-friendly non-toxic materials, there is ongoing efforts to develop Pb-free systems with comparable properties. In this context the discovery of the Pb-free solid solution of (1-x)$Na_{0.5}Bi_{0.5}TiO_3$-$x$$BaTiO_3$ (NBT-xBT) made a remarkable impact as it demonstrated seemingly MPB characteristics[2]. However later it was realized that the properties are not that promising as Pb-containing compounds and subsequently prompted a huge curiosity to understand its uniqueness in order to improve its efficiency as well as to develop new Pb-free systems.

The NBT-xBT solid solution exhibits an MPB around $x = 0.06$, where the enhancement of the piezoelectric effect was detected[2]. In contrast to the Pb-based systems, the MPB composition of NBT-xBT exhibits pseudocubic average symmetry and the amplification of the piezoelectric properties is not as strong as PZT or other Pb-based MPB systems[3,4]. Moreover the MPB was found quite unstable under external electric field[5–7] and mechanical stress[8] which induce irreversible structural transformations and successively shift the location of the MPB with respect to the virgin states. These various observations together with a number of theoretical studies[9,10] have implied that the system is likely to host multiple types of degenerate ferroelectric orders coupled with several competing local correlations, such as chemical ordering and octahedral tilts.

Evidently there have been many attempts over the years to provide deeper insights into the composition dependence of various mesoscopic-scale structural correlations in NBT-xBT[11–14]. However so far, the properties of NBT-xBT at the MPB have been qualitatively related to complex domain morphologies[5,15] and field-induced phase transitions which promote higher piezoelectric activity[16,17]. A recent study also proposed the presence of nanotwins with monoclinic symmetry facilitating rotation of the polarization under electric field around the MPB[18]. However neither of these observations nor the existing empirical understanding of the structure-property relationships can describe unambiguously the uniqueness of NBT-xBT, for instance, to what extent the popular models of polarization rotation and extension coupled with the free-energy instability can be applied to this system[19–21].

In this context, we have applied neutron total scattering and Raman scattering methods to examine exclusively the local structural features and the mechanisms of different atomic coupling processes across the MPB of

NBT-xBT at ambient conditions. We have adopted the so-called 'geometric phase approach'[22] to show explicitly how the local environment of each cation and the ensuing polarization develop as a function of composition. This has been achieved via analyzing pair distribution functions (PDFs) implementing the so-called 'big box' crystal modeling utilizing the reverse Monte Carlo (RMC) technique[23].

In the case of perovskite-type (ABO_3) dielectrics, the length-scale sensitivity of Raman spectroscopy is within a few unit cells, which nicely complements structural information provided by PDF analyses. Furthermore, the time-scale sensitivity of Raman spectroscopy is of the order of the period of atomic vibrations, thus giving us the opportunity to detect dynamic fluctuations with a lifetime $>\sim 10^{-11}$-10^{-12}s. Therefore, the composition development of the atomic dynamics revealed by Raman spectroscopy is indicative of atomic coupling processes occurring at the MPB whereby their relation to the exhibition of anomalous properties can be understood.

II. EXPERIMENTAL DETAILS

Ceramic samples of NBT-xBT with x = 0, 0.03, 0.04, 0.05, 0.06, 0.07, 0.08, 0.10, 0.15, and 0.20 were prepared following the typical solid state synthesis route which started from mixing the oxides in expected stoichiometric ratio by wet ball-milling in ethanol media for about 24 h. Three stages of heating with intermediate grinding were performed for each composition. Undoped NBT was first heated at 1073 K for 6 h, then at 1273 K for 4 h, and finally sintered at 1373 K for 2.5 h. The doped samples were calcined at 1173 K for 6 h and at 1323 K for 4 h. They were ultimately sintered at 1423 K for 2.5 h. The chemical compositions of the sintered samples were verified by wavelength-dispersive x-ray spectroscopy, using a Cameca Microbeam SX100 SEM-system. The results of the chemical analysis are shown in Fig. S1[24].

Room-temperature neutron total scattering data were collected at the NOMAD beamline in Oak Ridge National Laboratory. Fourier transformations of the corrected powder diffraction data were performed with a maximum Q of 31.4 Å^{-1}, which manifested a resolution of 0.1 Å in the real space. The general description regarding total scattering experiments and procedures to obtain the pair distribution functions (PDFs) can be found elsewhere[25]. The PDFs were modelled using the RMC method as implemented in the RMCprofile package[26]. In RMCprofile model structures were refined against both PDF (up to 20 Å) and total stricture factor F(Q) simultaneously, where the analytical expression of PDF follows the equation **26** and F(Q) follows the equation **11** as described in Ref[27].

In RMC iterations we have applied a distance-window constraint for each cation in order to make sure the refined structures remain rational, and also used the available swap utility for the A-site cations which allow to swap the positions among the three types of A-site cations randomly during the refinement to mimic the chemical disorder. For all compositions, the initial structural models were in pseudocubic setting with the box-size of approximately 54 Å× 54 Å× 54 Å, containing 13720 atoms. For each composition there were 30 independent runs in order to obtain good statistics.

The analysis of the refined structural models were done using the DISCUS package.[28] Following steps were adopted to extract the relative displacements ($\delta\vec{r}$) of the cation with respect to their oxygen environment:

1. The output structure file of each RMC calculation was first converted into a DISCUS-readable format.
2. All fractional atomic coordinates were then normalized with respect to the obtained average position of Bi cations so that the average site-coordinates of the Bi becomes nearly (0, 0, 0).
3. The coordinates of the neighboring oxygen atoms for each cation were extracted and averaged to obtain the geometric center of the oxygen polyhedra.
4. Difference between the normalized cation coordinates and the averaged oxygen coordinates provided the polar displacement vectors as follows:

$$\delta\vec{r}_A = \vec{r}_A - \frac{1}{12}\sum_i \vec{r}_{iO} \quad (1)$$

$$\delta\vec{r}_{Ti} = \vec{r}_{Ti} - \frac{1}{6}\sum_i \vec{r}_{iO} \quad (2)$$

$$\delta\widehat{r} = \frac{\delta\vec{r}}{|\delta\vec{r}|} \quad (3)$$

5. The directions of the displacement vectors were finally projected in a stereographic plot of a cubic crystal looking down $[001]_{pc}$.
6. The results from all 30 RMC runs were combined for each composition in order to increase the statistics of the structural information.

Room-temperature Raman scattering spectra were collected with a Horiba Jobin-Yvon T64000 triple-grating spectrometer equipped with an Olympus BH41 microscope and a 50x long-working distance objective on disc-shaped pellets of pressed powders in a backscattering geometry. The 514.5 nm line of an Ar^+ laser (Coherent 90C FreD) was used to excite the Raman scattering. No polarization, orientation, or spatial dependence of the Raman spectra was detected, indicating that the average linear crystallite size is smaller than the diameter of the laser spot on the sample surface, which was 2 μm. The measured spectra were temperature reduced by the Bose-Einstein phonon occupation factor: $I_{reduced} = I_{measured}/(n(\omega, T) + 1)$ with

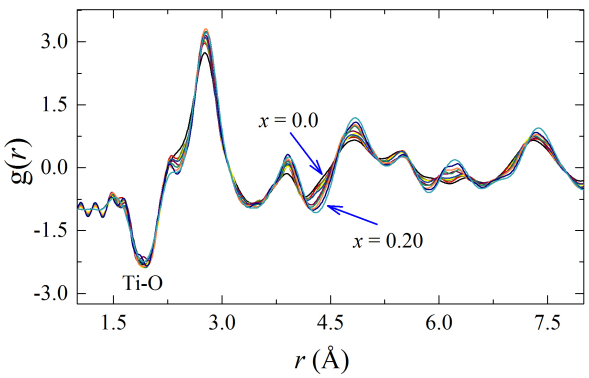

FIG. 1. Gradual development of the short- and intermediate-range PDFs for NBT-xBT as a function of composition. The analytical form of PDFs shown here is given by Equation **16** in the Ref.[27]

$n(\omega, T) = 1/(exp(\hbar\omega/kT) - 1)$, and then fitted with pseudo-Voigt peak-shape functions (PV = qL + (1-q)G, q ∈ [0, 1], L and G stand for Lorentzian and Gaussian, respectively) to determine the phonon wavenumbers ω, full-widths-at-half-maximum (FWHMs), integrated intensities I, and the Lorentzian weight coefficients q. The criterion for existence of a peak was $dI/I < 1$, where I and dI are the magnitude and the uncertainty of the integrated intensity, respectively.

III. RESULTS AND DISCUSSIONS

A. Pair distribution function analysis

PDFs describe structures in terms of weighted distributions of all possible atom-atom distances in a given system and thus allow direct analyses of short- and intermediate-range of atomic arrangements (see Fig.1). Here we have focused on the evolving oxygen environments of the cations, where A- and B-site cations are ideally surrounded by 12 and 6 oxygen atoms, respectively (Fig.2a). This enabled us to extract the characteristic polar displacements $\delta\vec{r}$ of the cations and their development as a function of composition. Quantitatively, the magnitude ($|\delta\vec{r}|$) is linked to the macroscopic polarization while the direction ($\delta\widehat{r} = \frac{\delta\vec{r}}{|\delta\vec{r}|}$) dictates the average symmetry of the system – given that in an unpolarized cubic state the positions of the A- and B-site cations coincide with the geometric centers of their respective oxygen polyhedra[22,29,30].

Figure 2b illustrates the directions of such relative displacements in [001] stereograms, which virtually describes the probabilistic trend of the atomic scale polar order and its evolution with compositions. The maps for undoped NBT with favored directions spread over a large area around [001] cannot be linked to a distinct average symmetry, instead they indicate the existence of several phases which potentially include low symmetry phases, but a significant fraction surely exhibits tetragonal-type displacement along $[001]_{pc}$. This complements thoroughly the reports on imaging local tetragonal distortions in pure NBT[31–33]. It is also apparent that the longstanding ambiguity in the crystallographic description of the average structure of undoped NBT[34–37] is merely a consequence of the disorder of $\widehat{r}$, which can manifest length-scale-dependent observations leading to modulated structural features[38–40]. Similarly the maps for the Ba doped NBT in the range $0.03 \leq x \leq 0.06$ conform to the reports suggesting distinct local and average polar order, and the coexistence of multiple phases[3,41–44]. Nevertheless, the preferences of $\delta\widehat{r}$ of A- and B-site Ti^{4+} at $x = 0.0$ is clearly changed on the onset of doping. This high sensitivity of the preferred directions of the host cations to Ba doping strongly supports the idea of inherent metastability of the ground state of unmodified NBT which can be altered irreversibly by thermal, mechanical or electrical stimulants[36], and further, the assumption of an additional phase boundary at $x = 0.03$[44,45] in NBT-xBT. Evidently, the stereographs at $x = 0.05$ stands out from the rest as they exhibit the largest areas with maximum probability and $x = 0.06$ truly presents the boundary before all the cations adopt well-defined tetragonal-type [001] distortions with increasing x.

Quantitative description of the stereographs can be realized via an orientation-order parameter $\xi = 1.5\langle\cos^2\theta\rangle - 0.5$ (Fig.3), where θ is the angle between $\delta\vec{r}$ and $[001]_{pc}$ and lies within -90° ≤ θ ≤ 90°. The averaging of $cos^2\theta$ was done with the point-density values from the stereograms as weights. The values of ξ signify the randomness of ionic displacements with respect to the chosen direction [001] and their development with x particularly when direction-distributions are more or less symmetric with respect to [001]. Evidently ξ manifests the minimum value for all cations around $x = 0.05$ and 0.06, suggesting the maximum stochasticity of the polar order within the system before all cations adopt predominantly tetragonal-type distortions with an increased length of correlations among them. The correlation-lengths can be anticipated from the spatial distribution of cosθ (0° ≤ θ ≤ 180°) in Fig.2(c) where cosθs for the A-site cations as a function of their unit-cell coordinates are mapped within one of the model boxes for each composition.

The mean polar displacements ($< |\delta\vec{r}| >$) of the cations as a function of composition along with their standard deviations are shown in Fig.4(b). As mentioned above, the relative displacements are directly linked to the inherent polarization of the system and ideally, a differential polarization can be estimated by the linear relationship:

$$\Delta P = \sum_i Z_i^* |\delta\vec{r}_i| \quad (4)$$

given that these displacements are calculated with respect to the center of the surrounding anions[22]. Therefore $< |\delta\vec{r}| >$ is a true representative of the spontaneous structural polarity of the material that can be associated with the macroscopic properties. Thus Fig.4b de-

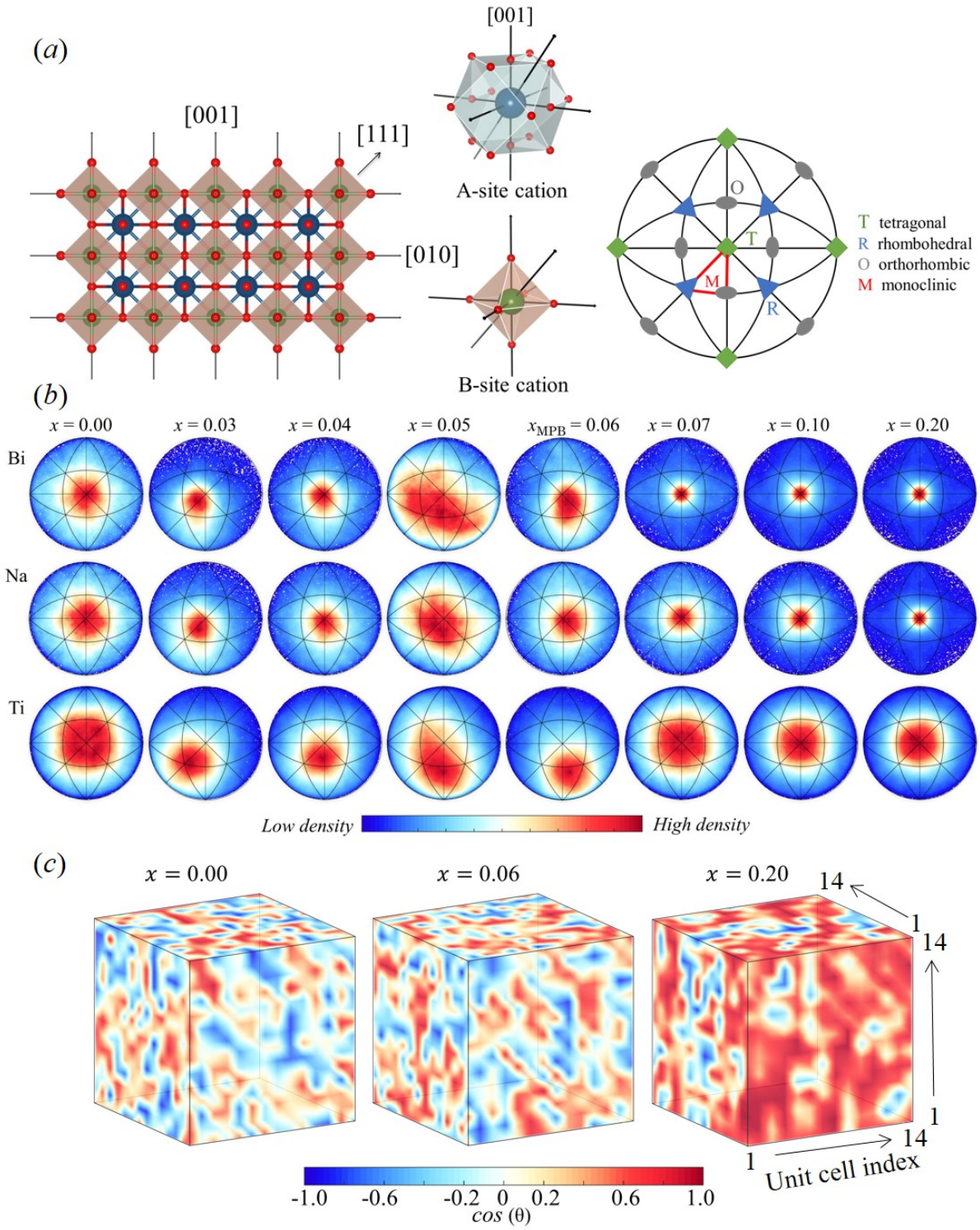

FIG. 2. (a) Schematic drawing of an aristotype cubic perovskite structure including different oxygen environments for A- and B-site cations. On the right is a guide [001] stereograph to identify the symmetry correspondence of the shift-directions ($\widehat{\delta r}$) shown below. Major pseudocubic directions ($\langle 001\rangle$, $\langle 110\rangle$ and $\langle 111\rangle$) have been marked with symmetry symbols, while the monoclinic mirror planes ($\{100\}$, and $\{110\}$) are shown in solid red lines. (b) Stereographs of $\widehat{\delta r}$ extracted from the refined big-box model structures as a function of composition. The colors follow the density distribution around each point on the graph, and therefore, help to visualize the statistical trend. (c) The variations of cosθ considering only A-site cations within one of the refined RMC configurations for selected compositions , where θ is the angle between $\delta\vec{r}_A$ and [001]. This virtually illustrates the spatial correlations of the polar displacements and their evolution with x. The model box for each composition has dimensions $\sim 54 \times 54 \times 54 \mathring{A}^3$.

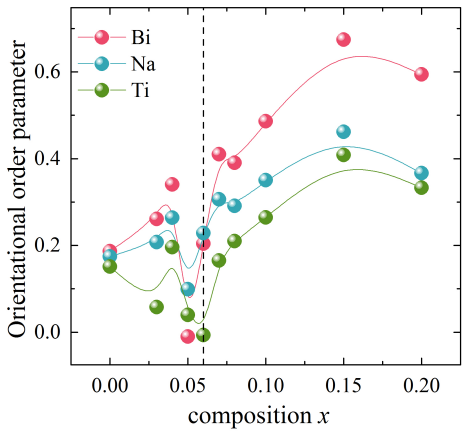

FIG. 3. Orientational order parameter ξ as a function of composition. Solid lines are simply guides to the eye. The dashed line marks the reported MPB composition[2]. Error bars are smaller than symbols.

scribes how the intrinsic polarization of NBT-xBT develops with the composition. It is obvious that the A-site cations have larger shifts than the B-site Ti^{4+} and the shifts in general remain almost unchanged in the range $0.0 \leq x \leq 0.06$. This hitherto undetected feature provides an important corollary: The overall structural polarity of the system remains unaffected by the variation of the composition in the range $x = 0.0$ - 0.06, from which it can be iterated that the amplification of the properties at the MPB cannot be exclusively governed by the so-called intrinsic factors[46]. Further implications of the above features are discussed later on, however one should make a few additional notes here: (1) The structural changes in the range $0.0 \leq x \leq 0.06$ are seemingly driven by an order-disorder phenomena; (2) the histograms of Bi displacements (Fig.3(a)) suggest that it has two distinguishable preferences at $x > 0.06$ as oppose to typical Gaussian distributions, which have resulted in an abrupt increase in $< |\delta\vec{r}| >$ as well as in sigmas, (3) the variation of $< |\delta\vec{r}| >$ with x classifies NBT-xBT as an A-site driven ferroelectric throughout the range $0.0 \leq x \leq 0.20$[47]; and finally, (4) the observed characteristics of Bi further call for comparative analysis with respect to Pb, including reviewing of the hypothesis that Bi can serve as a potential replacement of Pb in functional materials – which remains unclear to date.

Short-range chemical ordering has long been a controversial aspect in the discussion of local structures of NBT and NBT-based solid solutions. Although theoretical[9,10] and experimental[48,49] studies have shown evidences in support of A-site chemical ordering in undoped NBT, ambiguity still remains on the description of such ordering and its influences on the physical properties, especially at the MPBs of NBT-based solid solutions. In our refined models we have found a clear tendency to chemical ordering between Na and Bi as non-stoichiometric alternating layers along $[111]_{pc}$ in undoped NBT. However, the chemical ordering is progressively dislodged by the inclusion of Ba, which ultimately leads to local clustering of like atoms. In order to present this whole event quantitatively, we have calculated a pair correlation function as defined in the DISCUS package[50]:

$$c_{ij} = \frac{P_{ij} - \eta^2}{\eta(1-\eta)} \tag{5}$$

where P_{ij} denotes the total probability of sites i and j being occupied by the same type of atom, and η is the concentration of a cation in the system (see Fig.5). Negative values of c_{ij} refer to the situation where the sites i and j tend to be filled by different type of atoms while positive values indicate that sites i and j are more likely to be occupied by similar atoms . A correlation value of zero describes a random distribution. Hence, the MPB at $x = 0.06$ can be identified as the boundary where the likelihood of chemical ordering at the A site have been ceased for a critical amount of doping content.

The effect of chemical-ordering in the cationic displacements was conceived by calculating a displacement pair correlation function as follows[50]:

$$d_{ij} = \frac{\langle x_i x_j \rangle}{\sqrt{\langle x_i^2 \rangle \langle x_j^2 \rangle}} \tag{6}$$

Here x_i is the displacement of an atom on site i from the average position in a given direction. A positive d_{ij} refers to ferrodistortive (FD) correlations, whereas a negative value suggests antiferrodistortive (AFD) correlations, and a value around zero depicts a state without any correlations. Figure 6 shows the values of d_{ij} for all different A-site cation pairs, and it is evident that Bi-Bi pairs exhibit prominent AFD correlations at $x = 0.0$, which ultimately goes away with the chemical ordering above $x = 0.06$ and all pairs conform to FD correlations in the range $0.07 \leq x \leq 0.20$. Although it is well known that compounds of NBT and NBT-xBT exhibit antiferroelectric (AFE) features[16], here we exclusively reveal that AFE characteristics in NBT-based materials are driven by the antipolar displacements of Bi^{3+} cations.

Another important lattice instability of a perovskite-type structure is the tilting of the oxygen octahedra. Undoped NBT exhibits coherent tilting, which causes sharp superlattice reflections in the powder diffraction pattern[51]. From our big-box atomistic analyses, we tried to depict the disorder of the oxygen atoms through stereograms of their deviations with respect to the three orthogonal $\langle 001 \rangle$ directions as shown in the sketches of Fig.7. It is obvious that the oxygen atoms show a noticeable preference to have confinements along the one of the $\{001\}$ planes in the range $0.0 \leq x \leq 0.06$ in contrast to the symmetric distributions above $x = 0.06$, suggesting that MPB can also be seen as a point after which the system evolves to an untilted system from a tilted system.

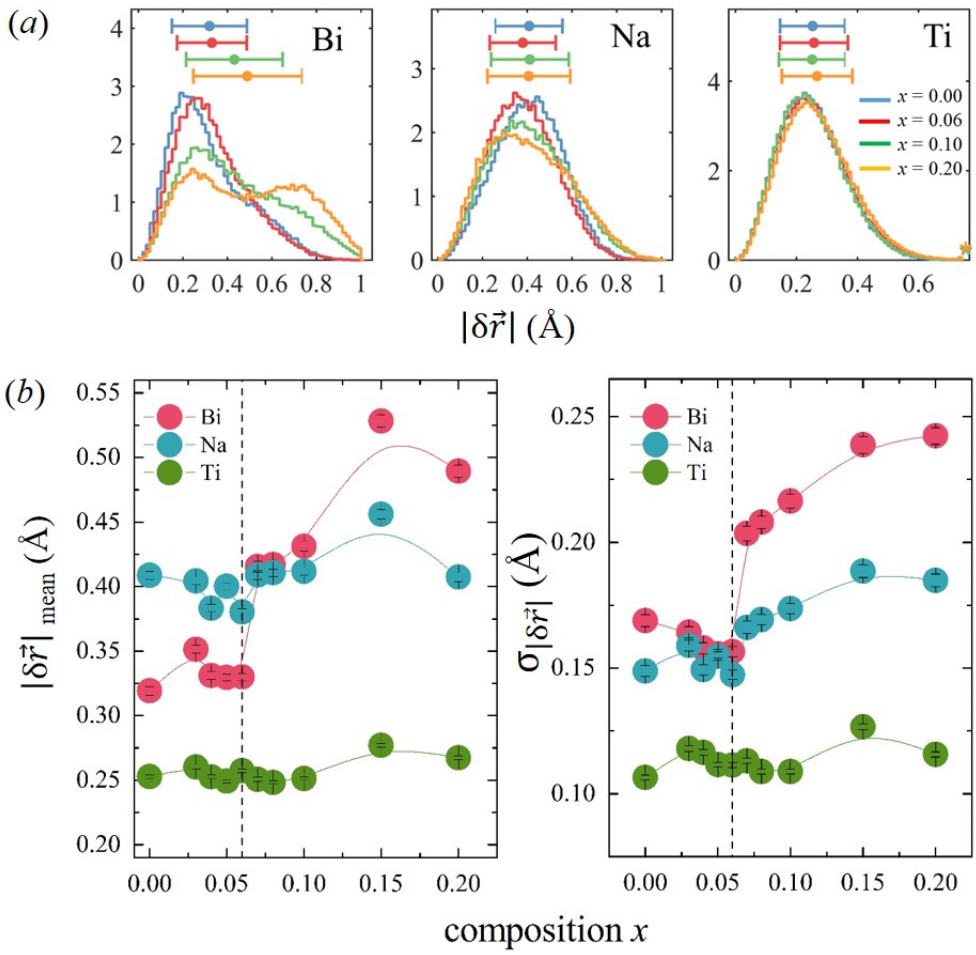

FIG. 4. (a) Probability distribution functions of the displacement magnitudes ($|\delta\vec{r}|$) as obtained from the refined models. Corresponding medians with their standard deviations are shown on the top of the distributions. Distinguishable changes in the distributions can be seen for the A-site cations with increasing x; Bi exhibits two distinct values of shifts with significant likelihoods for $x \geq 0.10$. Ti distributions remain unaltered with x. (b) Mean values of $|\delta\vec{r}|$ along with their corresponding standard deviations. Solid lines are mere guides to the eye, and error bars are smaller than symbols. The 'mean' values are representatives of the polarity of the system because $|\delta\vec{r}|$s are linear scale factors to the inherent polarization. σs quantify the inhomogeneities in polarity within the system.

The implications of the above observations of the chemical short-ranger order and the tilting of BO_6 octahedra with composition go beyond the mere validation of any of the previous assertions. Given the variation of the shifts in Fig.4(b), it can be well anticipated that the structural variation in the range $0.0 \leq x \leq 0.06$ are chiefly driven by competing local correlations, which happen to couple with the polarization and eventually affect the overall response functions. Our results clearly suggest that the strength of the various local coupling is significantly reduced by the chemical substitutions, and further indicate that these couplings basically act as barriers to the exhibition of better electromechanical properties in undoped NBT.

B. Raman scattering analysis

In the present context, Raman scattering data provide valuable information on the evolution of atomic dynamics as a function of x via phonon modes related to A- and B-site cations of an ABO_3 type perovskite structure. Quantitative details of different modes were extracted through a rigorous peak-fitting procedure following the peak assignments reported earlier[52–54] (see Fig. S7). Evidently, the MPB is revealed by the composition-driven development of the low-energy phonon modes involving A-site cation vibrations ω_1 and ω_2 around 40-60 cm^{-1}. In particular, as shown in Fig.8a, the components ω_1 and ω_2 merged into one for $x \geq x_{\mathrm{MPB}}$ and the average of the squared values, which effectively represent the strength of the interatomic interactions, has a minimum precisely

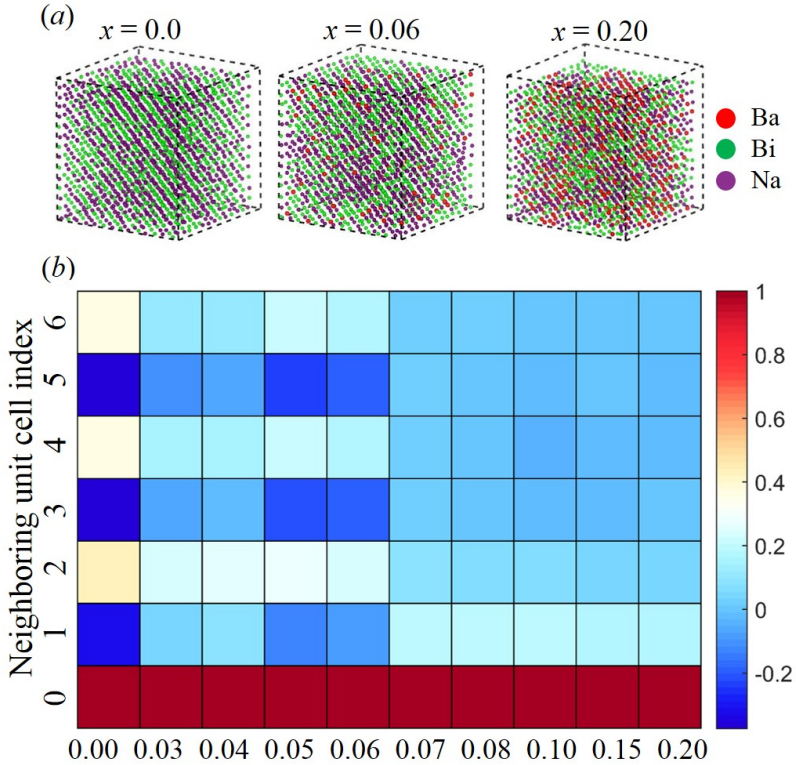

FIG. 5. (a) Crystal plots consisting only of A-site cations at three selected compositions. (b) The parameter c_{ij} (averaged over all refined configurations) shows the quantitative variation of the chemical ordering tendencies between Na and Bi including its length of correlation as a function of composition. The colors in the boxes represent specific values which can be estimated from the colorbar. The bottom row represents the self-correlation values, which is always 1.0. The alternating variation of the colors in the range $0 \leq x \leq 0.06$ signifies a alternating variation of negative and positive correlations values up to a six-unit-cell distance, hence suggests for chemical ordering. For compositions $x > 0.06$ the correlation parameter becomes positive for the first neighbors indicating possible clustering of like spices, which however gradually diminishes to zero (no correlation) with the increasing distances.

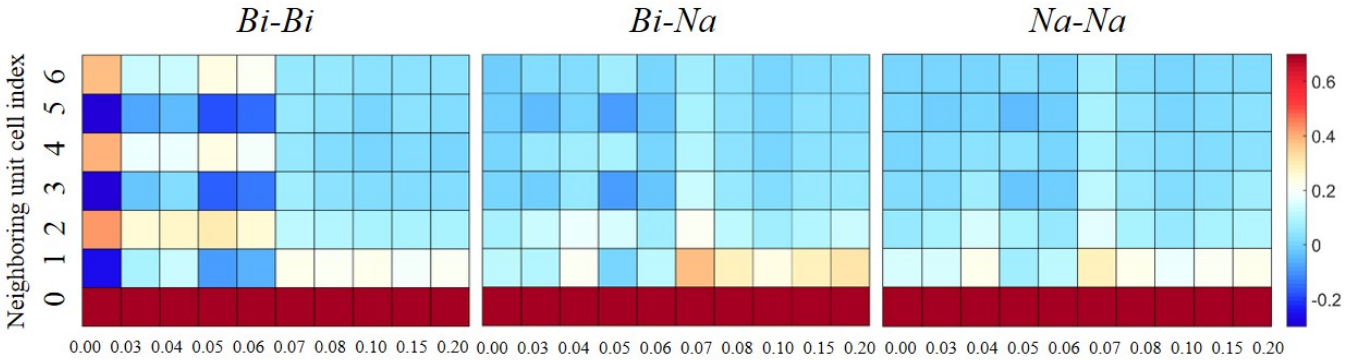

FIG. 6. Displacement pair correlation function d_{ij} averaged over all refined configurations for different pairs of A-site cations. The bottom row represents the self-correlation values, which is always 1.0.

at $x = 0.06$. The former signifies a reduction of the structural anisotropy, while the latter emphasizes the key role of the A-site cation rearrangements as the atomistic driving force for the composition-induced phase transition. These features can also be translated into a thermodynamical description that the local-potential barriers for the A-site cations become negligibly small with respect to the thermal fluctuations at different energy minimum. As a result, the multi-well potential functions transforms to a pseudo-isotropic function at $x = x_{\mathrm{MPB}}$. On con-

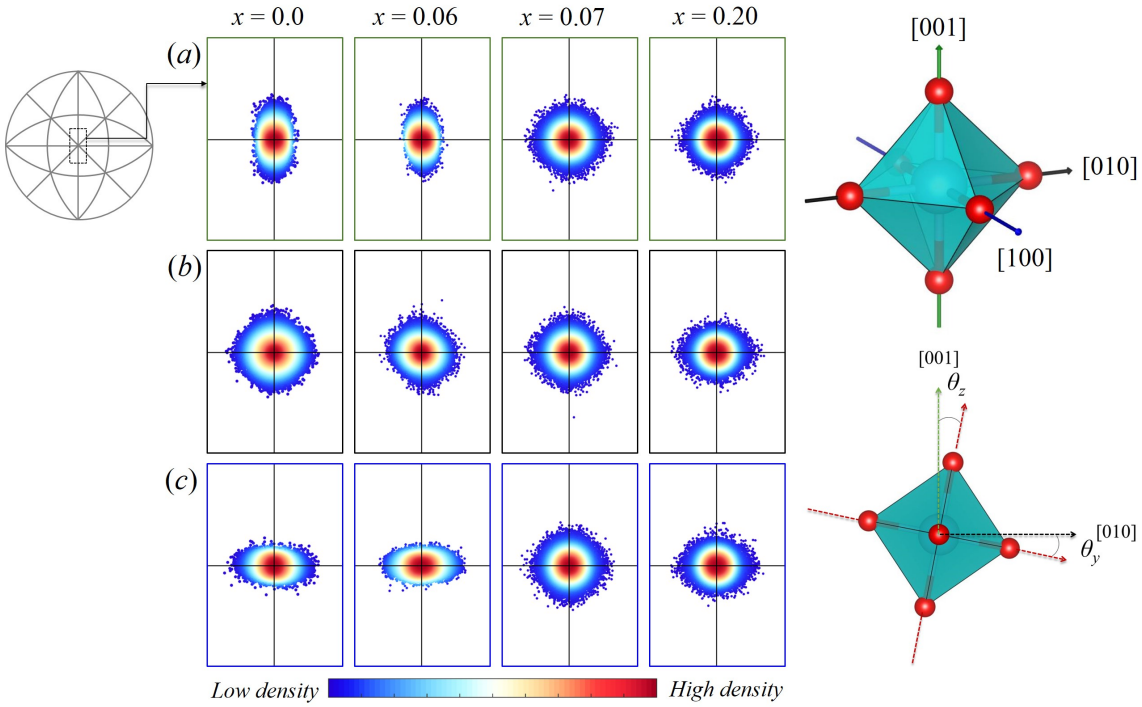

FIG. 7. Orientation preference of the apical oxygen atoms in the octahedra with respect to the three orthogonal ⟨001⟩ cubic directions. For each octahedra we obtained the three vectors joining the apical oxygen atoms along the orthogonal axes whose directions are then projected onto their respective (*a*) [001], (*b*) [010], and (*c*) [100] cubic stereographs. As such, for each octahedra three angles of deviation (θ_x, θ_y and θ_z) with respect to the corresponding orthogonal $< 001 >$ direction are obtained as shown in the schematic. Here the enlarged central regions of the graphs are shown for better visualization of the distributions.

trary, the dynamic states of the B-site Ti^{4+} cations remain anisotropic above x_{MPB}, as revealed by the persistence of two phonon energy states ω_4 and ω_5 in the entire range of composition studied here (Fig.8*d*). Therefore the local potential functions of the Ti^{4+} never become completely flat. Nevertheless the potential barriers are indeed reduced around the MPB since the difference factor between ω_4 and ω_5 decreases on the approach to the MPB composition (Fig.8*c*). Hence, one can deduce a sequence of the development of the local potential functions for different cations from the above results, as sketched in Fig.8*b*, and infer that the flattening of the energy functions are not perfect at the MPB here. Moreover, since the flattening does not come about uniformly for all types of cations, it can be anticipated that with the application of external stimuli, it is possible to stabilize the apparent structurally-frustrated system into one of its many degenerate ground states in the region $0.0 \leq x \leq 0.06$.

Finally, the softening of A-TiO_3 mode (Fig.8(*e*)), represented by the drop in ω_3 and the increase in the FWHM Γ_3, indicates a continuous enhancement in the dynamic coupling between the two subsystems of ferroelectrically active cations through the MPB. Obviously, the softening is not maximum at the critical composition $x = 0.06$. In fact, ω_3 shows a step-like change immediately after the MPB, and remains softer above the MPB in the range $0.06 < x \leq 0.20$. This has special significance considering the trends of d_{33} and K_t in Fig.9 including the reported behavior of the A-TiO_3 mode in the cases of Pb-containing solid solutions where the concurrence between the said dynamic coupling and the static structural instability has been proven to be a catalyzing condition for rendering better electromechanical properties[55,56].

IV. SUMMARY AND IMPLICATIONS

In summary, we have introduced a new paradigm to understand the composition-driven phase transition of NBT-xBT by revealing static and dynamic local structural characteristics beyond the conventional crystallographic information. The MPB was identified as a state consisting of an inherent random polarization instability with an increased dynamic coupling between the A-site and B-site subsystems which eventually give rise to enhanced electromechanical properties.

The enhancement of the physical properties for the Pb-based systems such as PZT, PMN-PT is normally understood in terms of easy rotation of the net polarization vector under external field, which entails the existence of a low-symmetry phase(s) together with the flattening of the Gibbs free energy function at the MPB[19,59].

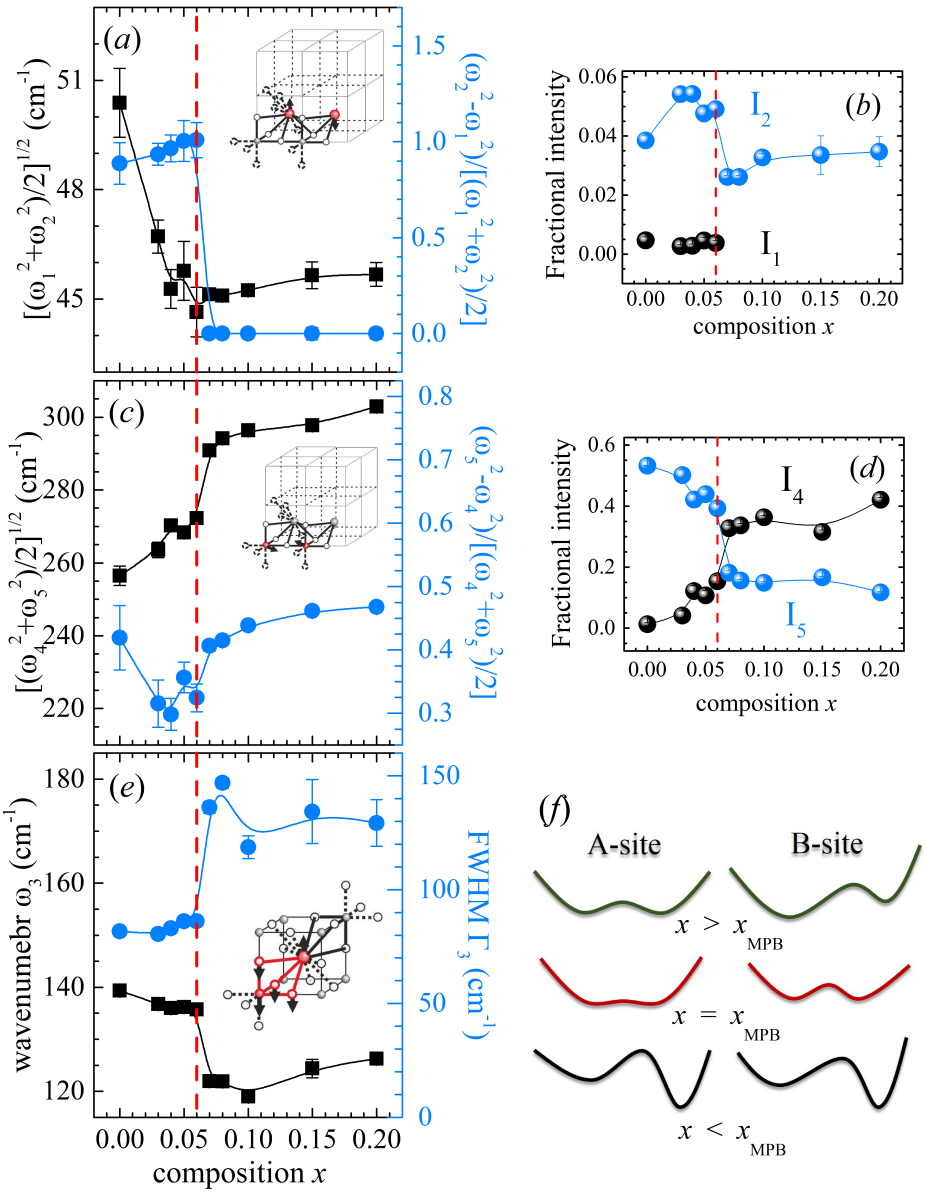

FIG. 8. Composition dependence of the average squared wavenumber and normalized split of Raman-active phonon modes comprising mainly Bi vibrations (a), Ti vibrations (c), and the wavenumber and FWHM of A-TiO_3 vibrations (e). In the case of two-component Raman scattering, the average squared wavenumbers were considered, which effectively represent the strength of corresponding interatomic interactions, and the normalized difference of squared wavenumbers, reflecting the anisotropy in the dynamical states. The fractional intensities of the modes comprising mainly vibrations of A-site (b) and B-site cations (d) represent the corresponding population of the energetically distinct states. The inserts of (a), (c) and (e) show sketches of the corresponding cubic phonon modes. (f) Schematic of the envisaged development of the local potential function of the A- and B-site cations with composition.

Clearly in the case of NBT-xBT the atomistic mechanism prompting the enhancement in the piezoelectric effect cannot be exclusively polarization-rotation or extension phenomena in the absence of low-symmetry phase(s) or polar-nonpolar instabilities. Our results underpin that it is rather a consequence of an enhanced flexibility or an easy switchability of the local dipoles in a strain-reduced environment where other competing factors, such as tilts, chemical ordering and AFD correlations, have been diminished by chemical tuning. Therefore, we propose that the elusive phase boundary of NBT-xBT around $x = 0.06$ at ambient conditions is a 'pseudo' MPB considering the fingerprints of an MPB in Pb-based systems.

In addition to the easy switching effect, the dynamic coupling between the A- and B-site cations can also be stated as an indispensable event to make the amplification of the piezoelectric properties to take place since the softening of ω_3 nicely matches with the relative increase

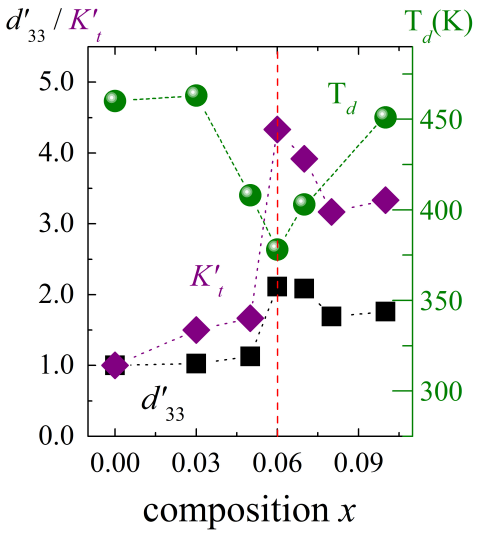

FIG. 9. Relative values of reported physical properties (piezoelectric coefficient d_{33}, electromechanical coupling factor K_t, and the depoling temperature T_d) with respect to the undoped NBT, obtained from the references Hiruma *et al.*[57] and Lidjici *et al.*[58].

of K_t and d_{33} (Fig.9. However the relative enhancement of the properties is not large because the intrinsic structural polarity is not improved and the structural instability does not translate to complete flattening of the local potential functions. The immediate drop of the relative d_{33} and K_t at $x = 0.07$ is indeed caused by an enhanced strain brought about by the increased structural polarity (Fig.4*b*). In fact the depolarization temperature (T_d) in Fig.9 also reiterates the polarization-strain decoupling consequences perfectly as a function composition.

In relation to the fundamental topic of providing efficient design principles, or how this 'pseudo' MPB can be transformed into a 'performing' MPB, our study demonstrates the importance of the local structural correlations of a system, rather than the symmetry of the average structure. The superior properties of the Pb-based systems including their wide range of thermal stability are arguably related to the affinity of Pb^{2+} to form electron lone pairs, which helps to maintain a strong intrinsic polarization at the A site along with the pivotal alliance between the static and the dynamic phenomena[30,55,56,60]. Furthermore, all Pb-based solid solutions with a giant piezoelectric response (e.g. PZT and xBiMeO$_3$-(1-x)PbTiO$_3$ systems with Pb partially substituted by Bi^{3+}) are B-site complex perovskites and the presence of a second type of B-site cation is expected to lower the potential barrier between different energetic states of the B-site cations. In fact we have recently reported that in the case of xBiMg$_{0.5}$Ti$_{0.5}$O$_3$-PbTiO$_3$ the inherent polarization does not decrease near the MPB, and there is concurrent flattening of the local potential functions of A- and B-site cations[55]. Hence the atomistic mechanism of achieving strong piezoelectricity should include flattening of the multi-well potential functions of both the A- and B-site cations together with a large inherent structural polarity. Therefore it suffices to say that Pb-free systems with giant piezoelectric response can hardly be designed by introducing chemical disorder only at the A site, even in the case of systems with Bi^{3+} having the same outer most electron shell as Pb^{2+}. We assume that local strains induced by unequal double doping of type $A'_xA''_{1-x}B'_yB''_{1-y}O_3$, such as $Na_xK_{1-x}Nb_yTa_{1-x})O_3$[61] and $(Ba_{0.7}Ca_{0.3})TiO_3$-$Ba(Zr_{0.8}Ti_{0.2})O_3$[62], should give rise to both essential effects.

ACKNOWLEDGMENTS

Financial support by the Deutsche Forschungsgemeinschaft (MI 1127/8-1) is gratefully acknowledged. A part of this research at ORNL's Spallation Neutron Source was sponsored by the Scientific User Facilities Division, Office of Basic Energy Sciences, U.S. Department of Energy.

* kaustuv.datta@uni-hamburg.de

[1] B. Jaffe, R. S. Roth, and S. Marzullo, J. Appl. Phys. **25**, 809 (1954).

[2] T. Takenaka, K.-i. Maruyama, and K. Sakata, Jpn. J. Appl. Phys. **30**, 2236 (1991).

[3] R. Garg, B. N. Rao, A. Senyshyn, and R. Ranjan, J. Appl. Phys. **114**, 234102 (2013), https://doi.org/10.1063/1.4842855.

[4] D. Damjanovic, N. Klein, J. Li, and V. Porokhonskyy, Funct. Mater. Lett. **03**, 5 (2010).

[5] W. Jo, J. E. Daniels, J. L. Jones, X. Tan, P. a. Thomas, D. Damjanovic, and J. Rodel, J. Appl. Phys. **109**, 014110 (2011).

[6] C. Ma, H. Guo, S. P. Beckman, and X. Tan, Phys. Rev. Lett. **109**, 107602 (2012).

[7] R. Garg, B. N. Rao, A. Senyshyn, P. S. R. Krishna, and R. Ranjan, Phys. Rev. B **88**, 014103 (2013).

[8] F. H. Schader, Z. Wang, M. Hinterstein, J. E. Daniels, and K. G. Webber, Phys. Rev. B **93**, 134111 (2016).

[9] M. Gröting, H. Silke, and K. Albe, J. Solid State Chem. **184**, 2041 (2011).

[10] M. Gröting, I. Kornev, B. Dkhil, and K. Albe, Phys. Rev. B **86**, 134118 (2012).

[11] P. Thomas, S. Trujillo, M. Boudard, S. Gorfman, and J. Kreisel, Solid State Sci. **12**, 311 (2010).

[12] J. E. Daniels, W. Jo, and W. Donner, JOM **64**, 174 (2012).

[13] W. Ge, C. P. Devreugd, D. Phelan, Q. Zhang, M. Ahart, J. Li, H. Luo, L. a. Boatner, D. Viehland, and P. M. Gehring, Phys. Rev. B **88**, 174115 (2013).

[14] P. B. Groszewicz, M. Gröting, H. Breitzke, W. Jo, K. Albe, G. Buntkowsky, and Rödel, Sci. Rep. **6**, 31739 (2016).

[15] J. Yao, N. Monsegue, M. Murayama, W. Leng, W. T. Reynolds, Q. Zhang, H. Luo, J. Li, W. Ge, and D. Viehland, Appl. Phys. Lett. **100**, 012901 (2012).

[16] Y. Guo, Y. Liu, R. L. Withers, F. Brink, and H. Chen, Chem. Mater. **23**, 219 (2011).

[17] W. Zeng, X. Zhou, J. Chen, J. Liao, C. Zhou, Z. Cen, T. Yang, H. Yang, Q. Zhou, G. Chen, and C. Yuan, Appl. Phys. Lett. **104**, 242910 (2014).

[18] D. Maurya, M. Murayama, a. Pramanick, W. T. Reynolds, K. An, and S. Priya, J. Appl. Phys. **113**, 114101 (2013).

[19] H. Fu and R. Cohen, Nature **403**, 281 (2000).

[20] D. Damjanovic, J. Amer. Ceram. Soc. **88**, 2663 (2005).

[21] M. Budimir, D. Damjanovic, and N. Setter, Phys. Rev. B **73**, 174106 (2006).

[22] R. Resta, Rev. Mod. Phys. **66**, 899 (1994).

[23] R. L. McGreevy, J. Phys. Cond. Matter **13**, R877 (2001).

[24] Supplemental Material [url] contains additional figures and Reference 25 and 27.

[25] T.Egami and S. Billinge, *Underneath the Bragg Peaks Structural Analysis of Complex Materials* (Pergamon Materials Series, 2012).

[26] M. G. Tucker, M. T. Dove, and D. A. Keen, J Appl. Cryst. **34**, 630 (2001).

[27] D. A. Keen, Journal of Applied Crystallography **34**, 172 (2001).

[28] R. B. Neder and T. Proffen, *Diffuse scattering and defect structure simulations - A cook book using the program DISCUS* (Oxford University Press, UK, 2007).

[29] I. Grinberg, V. Cooper, and A. Rappe, Nature **419**, 909 (2002).

[30] K. Datta, A. Richter, M. Göbbels, D. A. Keen, and R. B. Neder, Phys. Rev. B **93**, 064102 (2016).

[31] V. Dorcet and G. Trolliard, Acta Mater. **56** (2008), 10.1016/j.actamat.2007.12.027.

[32] R. Beanland and P. Thomas, Scripta Materialia **65**, 440 (2011).

[33] R. Beanland and P. A. Thomas, Phys. Rev. B **89**, 174102 (2014).

[34] S. Gorfman and P. A. Thomas, J. Appl. Cryst. **43**, 1409 (2010).

[35] E. Aksel, J. S. Forrester, J. L. Jones, P. A. Thomas, K. Page, and M. R. Suchomel, Appl. Phys. Lett. **98**, 152901 (2011).

[36] B. N. Rao, A. N. Fitch, and R. Ranjan, Phys. Rev. B **87**, 060102 (2013).

[37] R. R. McQuade and M. R. Dolgos, Journal of Solid State Chemistry **242**, 140 (2016), solid State Chemistry of Energy-Related Materials.

[38] A. M. Balagurov, E. Y. Koroleva, A. A. Naberezhnov, V. P. Sakhnenko, B. N. Savenko, N. V. Ter-Oganessian, and S. B. Vakhrushev, Phase Transitions **79**, 163 (2006).

[39] I. Levin and I. M. Reaney, Adv. Funct. Mater. **22** (2012), 10.1002/adfm.201200282.

[40] E. Aksel, Phys. Rev. B **87** (2013), 10.1103/PhysRevB.87.104113.

[41] B. Wylie-van Eerd, D. Damjanovic, N. Klein, N. Setter, and J. Trodahl, Phys. Rev. B **82**, 104112 (2010).

[42] F. Cordero, F. Craciun, F. Trequattrini, E. Mercadelli, and C. Galassi, Phys. Rev. B **81**, 144124 (2010).

[43] W. Jo, S. Schaab, E. Sapper, L. a. Schmitt, H.-J. Kleebe, A. J. Bell, and J. Rodel, J. Appl. Phys. **110**, 074106 (2011).

[44] C. Ma, H. Guo, and X. Tan, Adv. Funct. Mater. **23**, 5261 (2013).

[45] B. N. Rao, M. Avdeev, B. Kennedy, and R. Ranjan, Phys. Rev. B **92**, 214107 (2015).

[46] L. Bellaiche and D. Vanderbilt, Phys. Rev. Lett. **83**, 1347 (1999).

[47] M. Ghita, M. Fornari, D. Singh, and S. Halilov, Phys. Rev. B **72**, 054114 (2005).

[48] J. Kreisel, P. Bouvier, B. Dkhil, P. A. Thomas, A. M. Glazer, T. R. Welberry, B. Chaabane, and M. Mezouar, Phys. Rev. B **68**, 014113 (2003).

[49] Y. Yoneda, J. Korean Phys. Soc. **66**, 1339 (2015).

[50] T. Proffen, V. Petkov, S. J. L. Billinge, and T. Vogt, Zeitschrift fur Krist. **217**, 47 (2002), 0201428 [cond-mat].

[51] G. O. Jones and P. A. Thomas, Acta Cryst. **B58**, 168 (2002).

[52] E. Husson, Key Eng. Mater. **155-156**, 1 (1998).

[53] A.-M. Welsch, B. J. Maier, B. Mihailova, R. J. Angel, J. Zhao, C. Paulmann, J. M. Engel, M. Gospodinov, V. Marinova, and U. Bismayer, Z. Kristallogr. **226**, 126 (2011).

[54] K. Datta, A. Richter, M. Göbbels, R. B. Neder, and B. Mihailova, Phys. Rev. B **90**, 064112 (2014).

[55] K. Datta, R. B. Neder, J. Chen, J. C. Neuefeind, and B. Mihailova, Sci. Rep. **7**, 471 (2017).

[56] K. Datta, R. B. Neder, J. Chen, J. C. Neuefeind, and B. Mihailova, Phys. Rev. Lett. **119**, 207604 (2017).

[57] Y. Hiruma, K. Yoshii, H. Nagata, and T. Takenaka, Ferroelectrics **346**, 114 (2007).

[58] H. Lidjici, B. Lagoun, M. Berrahal, M. Rguitti, M. A. Hentatti, and H. Khemakhem, J. Alloys Compd. **618**, 643 (2015).
[59] R. Guo, L. E. Cross, S.-E. Park, B. Noheda, D. E. Cox, and G. Shirane, Phys. Rev. Lett. **84**, 5423 (2000).
[60] T. Egami, Annu. Rev. Mater. Res. **37**, 297 (2007).
[61] H. Tian, X. Meng, C. Hu, P. Tan, X. Cao, G. Shi, Z. Zhou, and R. Zhang, Sci. Rep. **6**, 25637 (2016).
[62] W. Liu and X. Ren, Phys. Rev. Lett. **103**, 257602 (2009).